AEC Computing and Applied Mathematics Center

AEC RESEARCH AND DEVELOPMENT REPORT

PHYSICS AND MATHEMATICS

NYO-2880

THERMALIZATION OF A FAST ION IN A PLASMA

by

Herbert C. Kranzer

December 18, 1959

Institute of Mathematical Sciences

NEW YORK UNIVERSITY
NEW YORK, NEW YORK

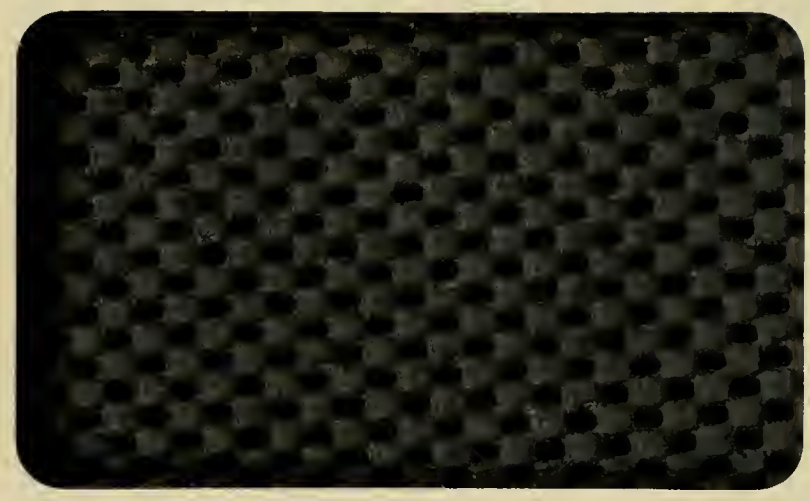

AEC COMPUTING AND APPLIED MATHEMATICS CENTER
Institute of Mathematical Sciences
New York University

PHYSICS AND
MATHEMATICS

NYO-2880

THERMALIZATION OF A FAST ION IN A PLASMA

by

Herbert C. Kranzer

December 18, 1959

Contract No. AT(30-1)-1480

Thermalization of a Fast Ion in a Plasma*

Herbert C. Kranzer

PREFACE

The question of the precise rate of thermalization of a fast ion in a plasma is of some interest in connection with several existing or proposed controlled thermonuclear devices. In this report, we follow a fast ion which is injected into a plasma in equilibrium. Specifically, we determine the time history of the probability distribution of this ion in velocity space. This is done by numerical integration of the linearized, space-independent Fokker-Planck equation with both the ion-ion and ion-electron interaction terms retained. The mean time of thermalization is calculated for several widely separated injection velocities. Some other properties of this single-ion probability distribution are analyzed.

The author is deeply indebted to H. Grad for initiating his interest in this problem and for many helpful suggestions along the way. He is grateful also for valuable discussions with R. Richtmyer and E. Isaacson concerning numerical procedures, and for the cooperation of M. Goldstein in making available the necessary computing time.

---

* This work was presented at an AEC - sponsored meeting on controlled thermonuclear fusion at Gatlinburg, Tennessee, April 27-28, 1959.

TABLE OF CONTENTS

1. The Physical Problem and its Differential Equations.

Suppose a single ion of velocity $\vec{\xi}_o$ is injected at time $t = 0$ into a homogeneous plasma in thermal equilibrium with no external electromagnetic fields present. The probability distribution $f(\vec{\xi}, t)$ of this ion in velocity space satisfies the space-independent Fokker-Planck equation[1]

$$\frac{\partial f}{\partial t} = - \frac{\partial}{\partial \xi_r} (a_r f) + \frac{\partial^2}{\partial \xi_r \partial \xi_s} (\frac{1}{2} b_{rs} f) \tag{1.1}$$

and the initial condition

$$f(\vec{\xi},0) = \delta(\vec{\xi} - \vec{\xi}_o). \tag{1.2}$$

(The convention of summation over repeated indices is employed.)

The values of the dynamical friction coefficient a_r and the dispersion coefficient b_{rs} to be taken in (1.1) are those corresponding to the (Maxwellian) distributions of ions and electrons in the original plasma.[2] This linearization is rigorously correct for a single injected ion.[3]

---

1. See Rosenbluth, MacDonald and Judd, Fokker-Planck Equation for an Inverse-Square Force, Phys. Rev., 107, 1 (1957), or Grad, Thermonuclear Reaction Rates in an Electrical Discharge, NYO-7977, Inst. of Math. Sciences, N. Y. Univ., Jan. 1958.

2. See Grad, op.cit., for the precise form of these coefficients in this case.

3. One can also consider f to describe the behavior of a "marked" ion in a plasma in equilibrium. In the more usual case where a whole group of ions is injected or "marked", our linearization amounts to ignoring the interaction between ions of this group as compared to the forces exerted by the plasma on the group as a whole. If one wants to include this mutual interaction, one has to take the values of a_r and b_{rs} corresponding to a linear perturbation of the Maxwellian distribution.

We introduce the dimensionless independent variables

$$\vec{x} = \vec{\xi}/(RT)^{1/2} , \tag{1.3}$$

$$\tau = \frac{4\pi n e^4 \ell n \Lambda}{M^{1/2}(kT)^{3/2}} t, \tag{1.4}$$

where T is the plasma temperature (assumed the same for electrons and ions), M is the ion mass, k is Boltzmann's constant, $R = k/M$, e is the electronic charge, n the number density of ions or electrons, and

$$\Lambda = \frac{3}{2} \frac{(kT)^{3/2}}{\sqrt{\pi n}\, e^3} \tag{1.5}$$

is the ratio of the Debye length to the mean distance of closest approach in a Coulomb encounter. (All quantities are expressed in cgs electrostatic units.) Then equations (1.1) and (1.2) become conditions

$$\frac{\partial \phi}{\partial \tau} = - \frac{\partial}{\partial x_r} (\alpha_r \phi) + \frac{\partial^2}{\partial x_r \partial x_s} (\tfrac{1}{2} \beta_{rs} \phi), \tag{1.6}$$

$$\phi(\vec{x},0) = \delta(\vec{x} - \vec{x}_o) , \qquad \vec{x}_o = \vec{\xi}_o/(RT)^{1/2} , \tag{1.7}$$

on the dimensionless probability distribution

$$\phi(\vec{x},\tau) = (RT)^{3/2} f(\vec{\xi},t). \tag{1.8}$$

Denoting by ρ^2 the ratio of ion mass to electron mass, the coefficients in (1.6) are given (for singly charged ions) by

$$(1.9)\qquad \begin{cases} \alpha_r = \alpha_r^+ + \alpha_r^- , \\ \beta_{rs} = \beta_{rs}^+ + \beta_{rs}^- , \end{cases}$$

with

$$(1.10)\qquad \begin{cases} \alpha_r^+ = -\,2\sqrt{\frac{2}{\pi}}\,\frac{x_r}{x^2}\,F(x), \\ \alpha_r^- = -\sqrt{\frac{2}{\pi}}\,(\rho + \rho^{-1})\,\frac{x_r}{x^2}\,F(\tfrac{x}{\rho}) , \end{cases}$$

$$(1.11)\qquad \beta_{rs}^{\pm} = \gamma_1^{\pm}\,\frac{x_r x_s}{x^2} + \gamma_2^{\pm}\,(\delta_{rs} - \frac{x_r x_s}{x^2}) ,$$

where

$$(1.12)\qquad \begin{cases} \gamma_1^+ = \sqrt{\frac{2}{\pi}} \cdot \frac{2}{x^2}\,F(x), \\ \gamma_1^- = \sqrt{\frac{2}{\pi}} \cdot \frac{2\rho}{x^2}\,F(\tfrac{x}{\rho}) , \end{cases}$$

$$(1.13)\qquad \begin{cases} \gamma_2^+ = \sqrt{\frac{2}{\pi}}\,[F(x) + \frac{F'(x)}{x}] , \\ \gamma_2^- = \sqrt{\frac{2}{\pi}}\,[\frac{1}{\rho}\,F(\tfrac{x}{\rho}) + \frac{1}{x}\,F'(\tfrac{x}{\rho})] \end{cases}$$

and

$$(1.14)\qquad F(x) = \frac{1}{x}\int_0^x e^{-y^2/2}dy - e^{-x^2/2}.$$

Our ultimate goal is to numerically integrate (1.6), (1.7), a system involving two velocity dimensions (there is axial symmetry about the direction of $\vec{x}_o$) and one time dimension.

In this report we assume spherical symmetry in velocity space, thus reducing the number of dimensions by one and rendering the problem more amenable to numerical treatment by a computer of finite size. If we are interested in following only the speed of the injected test ion, this should be an excellent approximation.

Hence we introduce the spherical mean value

$$(1.15) \qquad \frac{1}{x^2} \int\limits_{|\vec{y}|=x} \int \phi(\vec{y},\tau)\, d\omega_y = g(x,\tau)$$

and obtain for g the differential equation

$$(1.16) \qquad \frac{\partial g}{\partial \tau} = \sqrt{\frac{2}{\pi}} \cdot \frac{1}{x^2} \frac{\partial}{\partial x} \left(xGg + G \frac{\partial g}{\partial x} \right)$$

and the initial condition

$$(1.17) \qquad g(x,0) = x_o^{-2}\, \delta(x - x_o).$$

The function G = G(x) is defined as

$$(1.18) \qquad G(x) = F(x) + \rho F\left(\frac{x}{\rho}\right).$$

2. The Numerical Scheme

We proceed to the numerical solution of (1.16), (1.17) by finite differences. We approximate (1.16) by an explicit difference equation; i.e., we take a rectangular mesh with a spacing Δx in velocity and $\Delta\tau$ in time and replace $\frac{\partial g}{\partial \tau}$ by a forward difference. We use the same Δx throughout our mesh, even though the coefficients vary much more slowly when x is large, since the particular solutions we seek may vary rapidly with velocity for large x, particularly at early times.

To reduce truncation error, the right-hand side of (1.16) is first expanded into the form

$$(2.1) \qquad \frac{\partial g}{\partial \tau} = \sqrt{\frac{2}{\pi}} \cdot \frac{1}{x^2}\left[(xG' + G)g + (G' + xG)\frac{\partial g}{\partial x} + G\frac{\partial^2 g}{\partial x^2}\right].$$

$$= C(x)g + A(x)\frac{\partial g}{\partial x} + B(x)\frac{\partial^2 g}{\partial x^2}.$$

The x - derivatives of g in (2.1) are then replaced by centered differences, while the coefficients A, B, C are evaluated analytically. Because A(x) becomes infinite at $x = 0$, the first velocity mesh point is taken at $x = \frac{1}{2}\Delta x$; differences centered at this point are computed by assuming g to be an even function of x. The truncation error of this scheme is of the order of $(\Delta t)^2$ or $(\Delta x)^4$.

Since the maximum of $x^{-2}G$ occurs at $x = 0$ and is equal to $\frac{1}{3}$, the Courant-Friederichs-Lewy stability criterion (based on the $\frac{\partial^2 g}{\partial x^2}$ term alone) is satisfied if

$$(2.2) \qquad \lambda = \frac{\Delta\tau}{(\Delta x)^2} \leq \frac{3}{2}\sqrt{\frac{\pi}{2}} \approx 1.88.$$

For safety, we choose $\lambda = 1.75$. The full von Neumann stability criterion is then satisfied at all velocity points except the single point $x = \frac{1}{2}\Delta x$. This exception can be tolerated, since an oscillatory instability must have a wave length embracing at least two mesh points. We thus expect the solution of the difference equation to be stable as $\Delta\tau$ approaches zero.

Incidentally, this does <u>not</u> mean that numerical oscillations cannot develop. In fact, the use of a centered difference for $\frac{\partial g}{\partial x}$ will cause oscillations whenever the effect of the "drift" term $A\frac{\partial g}{\partial x}$ in one time cycle dominates that of the "diffusion" term $B\frac{\partial^2 g}{\partial x^2}$, i.e., whenever

$$(2.3) \qquad 2A^2\Delta\tau > B.$$

For reasonable values of $\Delta\tau$, inequality (2.3) holds when x is of the order of ρ (test ion speed $\sim$ mean plasma electron speed). In the one case that we consider in which such large values of x enter, oscillations are indeed observed at early times. What the von Neumann condition <u>does</u> insure is that any oscillations which do develop damp out as τ increases. This is exactly what does happen.

In most of the cases considered below, the initial values (1.17) of g are represented numerically by choosing x_o to coincide with a mesh point and taking $g(x,0)$ to be $x_o^{-2}(\Delta x)^{-1}$

at this mesh point and zero at the others. In the one case where $x_o > \rho$, this prescription would cause the oscillations mentioned in the preceeding paragraph to reach unacceptably large amplitudes before damping out. In this case, we begin the calculation at a time $\hat{\tau} > 0$ which is small relative to the time scale of thermalization. The starting values of g are chosen to be the values g would have at time $\hat{\tau}$ if the coefficients A, B, C in (2.1) had everywhere the values they have at x_o:

$$(2.4) \qquad g(x,\hat{\tau}) = \frac{\exp\left[C\hat{\tau} - (x-x_o+A\hat{\tau})^2/4B\hat{\tau}\right]}{2x_o^2(\pi B\hat{\tau})^{1/2}} .$$

The choice of numerical upper bounds for x and τ is facilitated by the fact that the exact solution of (1.16), (1.17) approaches as $\tau \longrightarrow \infty$ the Maxwellian distribution

$$(2.5) \qquad g_M(x) = \sqrt{\frac{2}{\pi}}\, e^{-x^2/2} .$$

Thus for an x not much larger than x_o the solution remains altogether negligible for all time. We take such an x for an outer boundary and impose there the artificial boundary condition g = 0. The upper bound on τ is determined by the computation itself: we stop computing whenever $g(x,\tau)$ is as close to $g_M(x)$ as the numerical approximation allows.

3. Injection Velocities and other Parameters.

Numerical computations have been performed for a plasma consisting of deuterium, for which $\rho = 60.5948$. Four widely spaced injection valocities x_o were chosen: $x_o = 0$, $x_o = 1.55$, $x_o = 9.7$, and $x_o = 240$. The first of these was chosen to provide a reference relaxation time. The second corresponds to the center of the initial distribution used by Rosenbluth's group[4] in a Fokker-Planck equation calculation of the thermalization of a group of test ions in the absence of an external plasma. The choice of the last two injection velocities can be most easily understood by reference to the "friction curve" -- the plot of the total friction coefficient α (cf. (1.6)) as a function of x (see Fig. 1). This curve begins at zero (for $x = 0$), rises to a maximum value α_M at about $x = 1.3$, decreases to a minimum at $x = 9.7$, rises to a second maximum value $\frac{1}{2}\alpha_M$ at $x = 1.3\rho \sim 80$, and finally falls off toward zero in proportion to x^{-2}. The velocity $x = 9.7$ lies at the central minimum, while $x = 240$ is approximately that velocity for which α reaches on its final downward curve the value that it has at $x = 9.7$.

The velocity mesh width Δx must be taken small enough to yield a significant number of points in the region $0 \leq x \leq 1.3$ in which α rises to its first maximum. This is also the region in which coefficients β_{rs} (particularly β^{+}_{rs}),

4. MacDonald, Rosenbluth, and Chuck, Relaxation of a System of Particles with Coulomb Interactions, Phys. Rev., 107, 350 (1957).

as well as the limiting solution $g_M(x)$, are substantially different from zero. Therefore, Δx was never chosen larger than 0.1.

The case $x_o = 240$ requires smoothing of the initial data, as described in Section 2. The time $\hat{\tau}$ of smoothing (see (2.4)) was taken as 37.7.

The numerical parameters used in the four cases are summarized in Table I. The computations were performed on the IBM 704 at New York University.

Injection velocity x_o	0	1.55	9.7	240
Initial smoothing time $\hat{\tau}$	0	0	0	37.7
Velocity mesh Δx	0.1	0.05	0.06	0.1
Time mesh $\Delta\tau$	0.0175	0.004375	0.0063	0.0175
Upper velocity bound x_{max}	7.0	7.0	12.0	250

Table I – Details of the numerical computation

4. The Numerical Results.

In the three cases where x_o is positive, the solutions behave quite similarly (see Fig. 2). At first, the initial delta-function diffuses into an asymmetric Gaussian distribution of varying width, steeper on the high-velocity side (Fig. 2A). The peak of this distribution migrates toward lower velocities (Fig. 2B). This regular evolution continues until the inner tail of the Gaussian reaches x = 0 (Fig. 2C). At that time, a second peak forms at x = 0 (Fig. 2D). This peak rapidly increases in height and width (Fig. 2E), completely swallowing up the original Gaussian, until (Fig 2F) it somewhat surpasses the Maxwellian distribution (2.5). Finally (Fig. 2G) it slowly falls back and broadens, approaching (2.5) asymptotically.

When $x_o = 0$, the initial distribution is just an extreme case of the pattern of Figure 2F. Hence the asymptotic decay toward the Maxwellian distribution begins immediately.

We proceed to give quantitative details of this general picture in the various cases. A physical idea of the size of the units involved may be obtained by noting that the root mean square plasma ion speed corresponds to $x = \sqrt{3} \approx 1.73$, while the r.m.s. electron speed corresponds to $x = \rho\sqrt{3} \approx 105$. Furthermore, the Spitzer ion-ion collision time[5]

$$(4.1) \qquad t_c = M^{1/2}(3kT)^{3/2} / 8 \times 0.714\ \pi n e^4 \ell n \Lambda$$

corresponds to $\tau = 3.62$.

---

5. Spitzer, Physics of Fully Ionized Gases, Interscience, New York, 1955.

The early stage of thermalization (through Fig. 2C) may best be understood by reference to the solution (2.4) of the equation obtained from eq. (2.1) by making its coefficients constant. This solution represents an exact (symmetric) Gaussian distribution whose width is proportional to $\sqrt{B\tau}$ and whose peak moves toward lower values of x with the constant speed A. Since the actual coefficients in (2.1) vary slowly with x, at least for $x > 1.3$, it is not surprising that the correct solution turns out to be approximately Gaussian at early times. Indeed, the motion of the peak toward lower x takes place with an instantaneous speed which is approximately equal to the value of A at the instantaneous position of this peak. (See Fig. 3, where the maxima and minima of the friction curve are clearly mirrored in the slopes of the peak-x-versus-τ curves.)

Even the slight asymmetry of the solution can be explained on this basis. One need only observe that B(x) is a monotone decreasing function of x, so that the distribution should have a greater "width" to the left of its peak than to the right.

In Figure 4, we plot the width (distance between half-peak points) of the solution as a function of the position of the peak in two of our cases. Note that the width does not depend simply on the monotone dispersion β, but rather seems to vary with the friction coefficient (or perhaps with $d\beta/dx$). Note furthermore that in both cases shown, especially in the case $x_o = 240$, the peak width in the early stages

surpasses the ultimate width $2\sqrt{2\ell n 2} \approx 2.4$ of the limiting Maxwellian distribution $g_M(x)$.

The graphs in Figures 3 and 4 are changed to dotted lines at the time $\tau = \tau_1$ when the central peak of Fig. 2D begins to form. They are cut off completely at $\tau = \tau_2$, the time at which the original peak no longer exists (between Figs. 2E and 2F). We call period $\tau_1 < \tau < \tau_2$, during which the central portion of the Maxwellian distribution (2.5) is filled out, the middle stage of thermalization. In Figure 5 we show the heights of the central peaks as a function of time during this middle stage and continuing on to (and in some cases beyond) the time $\tau = \tau_4$ defined below.

The late stage of thermalization, beginning at $\tau = \tau_2$, is characterized by the asymptotic decay of the solution toward the Maxwellian distribution $g_M(x)$. From physical reasoning (cf. Spitzer[5]), it is plausible to expect that this decay becomes exponential at late times. Accordingly, we compute numerically the average deviation

$$\sigma(\tau) = \int_0^\infty x^2 |g(x,\tau) - g_M(x)| \, dx \tag{4.2}$$

of the solution from Maxwellian and plot this deviation against time on a semilogarithmic graph (Figure 6). We observe that, in all four cases, this graph approximates a straight line from some time $\tau = \tau_3 > \tau_2$ on to quite late times. Thus we can conclude that there exists in each case a "relaxation time" $\tilde{\tau}$ such that

(4.3) $\sigma(\tau) = \text{const. } e^{-\tau/\tilde{\tau}}$ for $\tau > \tau_3$.

(The aberrations in the graphs of Figures 6A and 6B at very late times are due to purely numerical causes: $\sigma(\tau)$ becomes less than the truncation error. The leveling off in Figures 6C and 6D represents the filling out of the Maxwell tail.)

We define the mean time τ_4 of thermalization of an ion to be the time at which the average deviation of $g(x,\tau)$ from a Maxwellian distribution is 20 percent (i.e., $\sigma = 0.2$). The times τ_1, τ_2, τ_3, τ_4, $\tilde{\tau}$ are summarized in Table II. In the case $x_o = 240$, the smoothing time $\hat{\tau}$ is included in all elapsed times.

Also shown in Table II is the maximum deviation, due to truncation and roundoff errors, of the total number of test particles

(4.4) $$\int_0^\infty x^2 g(x,\tau)\, dx$$

from its theoretical value 1 during the time $0 \leq \tau \leq \tau_4$. The small size of these deviations is an indication of the accuracy of the computation.

Injection velocity x_o	0	1.55	9.7	240
Time τ_1, at which central peak begins to form	—	0.9	50	1840
Position x of outer peak at time τ_1	—	1.07	7.08	11.75
Time τ_2, at which outer peak disappears	—	1.3	100	1970
Position x of outer peak at time τ_2	—	0.82	3.90	4.2
Height g of outer peak at time τ_2	—	0.55	0.013	0.0085
Time τ_3, at which exponential decay begins	0	3.9	150	1990
Relaxation time $\tilde{\tau}$ of exponential decay	3.4	6.7	16	23
Mean thermalization time τ_4	6.0	4.4	157	2043
Ratio of τ_4 to Spitzer collision time	~ 2	~ 1.2	~ 45	~ 575
Maximum deviation of particle number from unity (up to time τ_4)	.001	10^{-5}	.001	.004

Table II - Principal numerical results

5. Conclusions.

The thermalization times given in Table II were the main goal of this investigation. Several other points also deserve mention, however.

First, some trivial observations. It seems clear from the slope of the curve in Fig. 3A that an ion whose speed $x \gg 9.7$ is slowed down principally by encounters with electrons, while for $x \ll 9.7$ it is the other ions that do the job. For $x \approx 9.7$, both are important. Furthermore, Fig. 4 shows that an ion is extremely unlikely to gain energy unless it is already below the mean energy of the plasma particles.

Secondly, no surprise should be occasioned by the difference in the relaxation times $\tilde{\tau}$ in the various cases. The relaxation time for $x_o = 0$ agrees fairly well with the Spitzer collision time. The other relaxation times are longer because the corresponding distributions are broader when they start to relax (see line 4 of Table II). Thus the Spitzer collision time cannot be taken as an absolute measure of the rate of approach to equilibrium.

Of course, the existence of an exponential decay toward a Maxwellian distribution does not contradict Rosenbluth's observation[4] that the Maxwell tail takes infinitely long to fill up. The reason, as (4.2) shows, is that the tail makes a contribution to the deviation $\sigma(\tau)$ which decreases faster than exponentially. In fact, the point $x = X$ of the tail is weighted with a factor $\sqrt{\frac{2}{\pi}}\, X^2 e^{-X^2/2}$ in the computation of σ.

Finally, it is instructive to compare our numerical solution in the case $x_o = 1.55$ with the solution of Rosenbluth mentioned in Section 3 above. This comparison, made in Table III, shows a qualitative similarity in the mode of thermalization in these two extremely different situations. The speed of thermalization, however, is almost twice as great in the present calculation. In other words, if a group of ions, originally all at the same speed ξ, come to Maxwellian equilibrium under the forces between them in time T, then an ion injected with velocity ξ into the resulting plasma will thermalize (i.e., attain a Maxwellian velocity distribution) in a time slightly greater than T/2.

Source	This report, $x_o = 1.55$	MacDonald, Rosenbluth, and Chuck[4]
External plasma present	yes	no
τ_1	0.9	1.5
x of peak at τ_1	1.07	1.03
τ_2	1.3	1.75
$\tilde{\tau}$	6.7	11 (estimated)

Table III - Comparison of time scales of thermalization in the presence and absence of an external plasma.

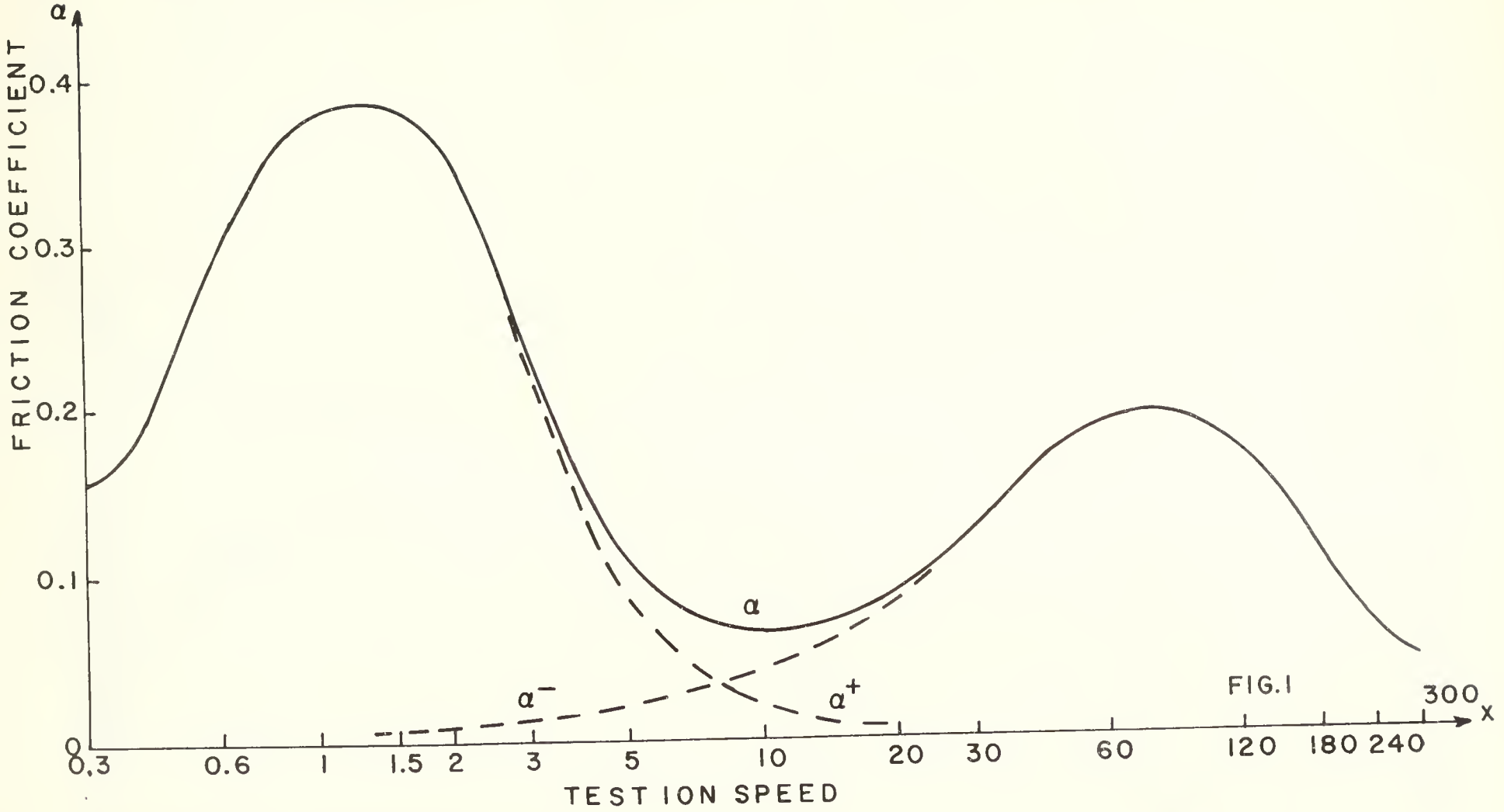
α
FRICTION COEFFICIENT
0.4
0.3
0.2
0.1
0
α
α⁻
α⁺
0.3
0.6
1
1.5
2
3
5
10
20
30
60
120
180
240
300
X
TEST ION SPEED

FIG.1

FIG. 2: SUCCESSIVE STAGES OF THERMALIZATIO

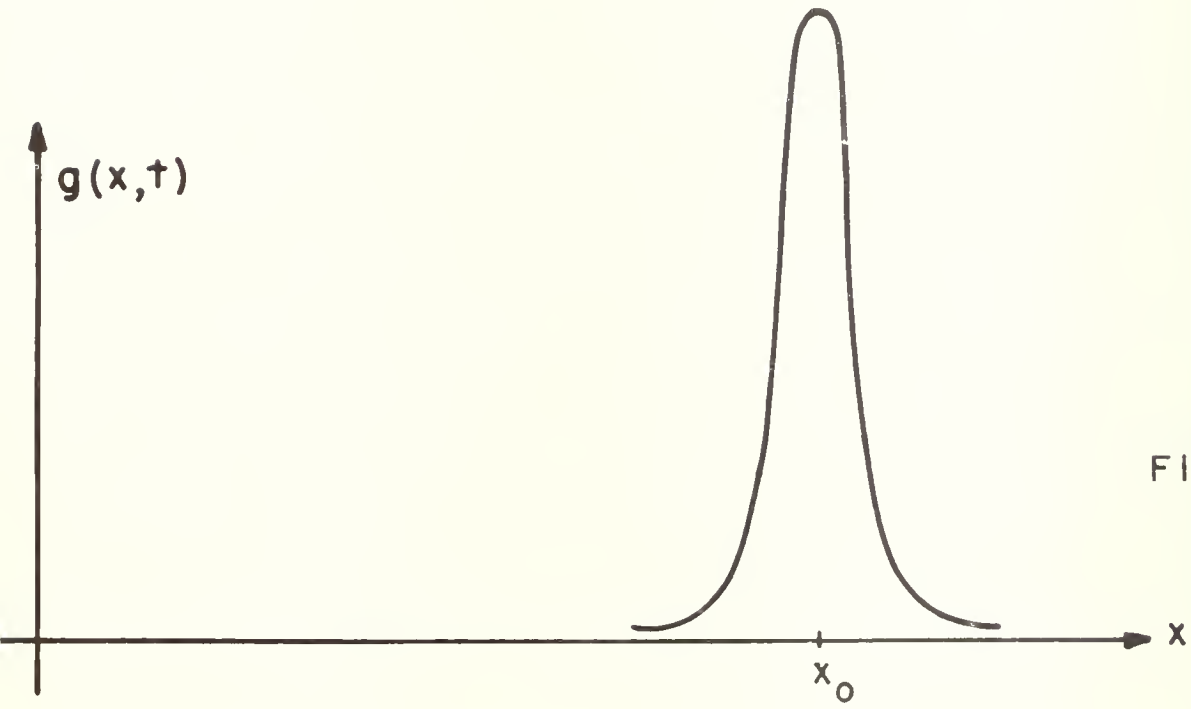

FIG. 2A

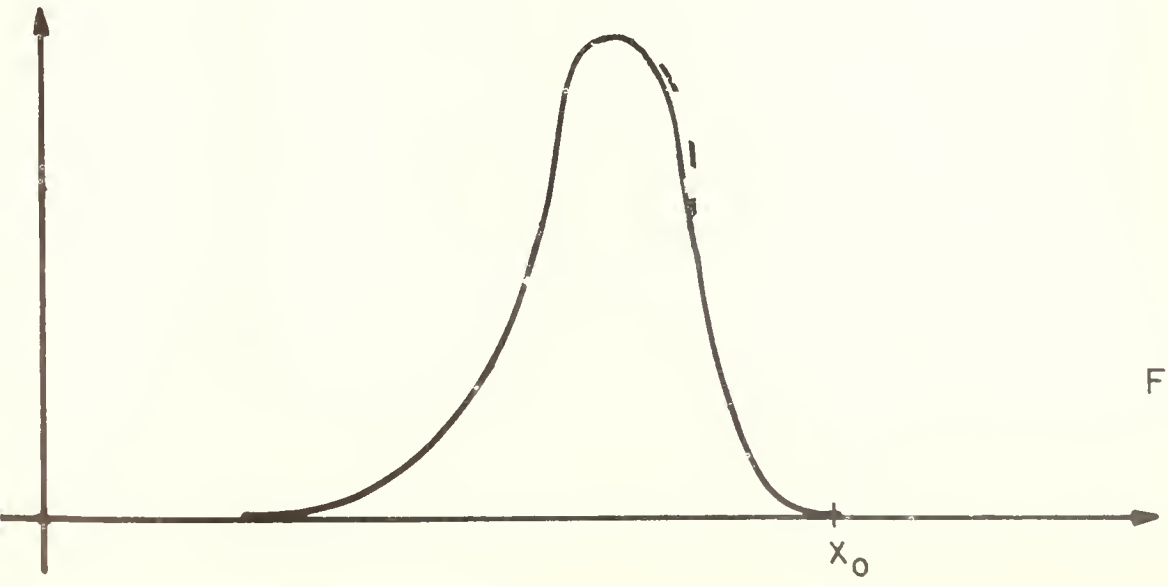

FIG. 2B

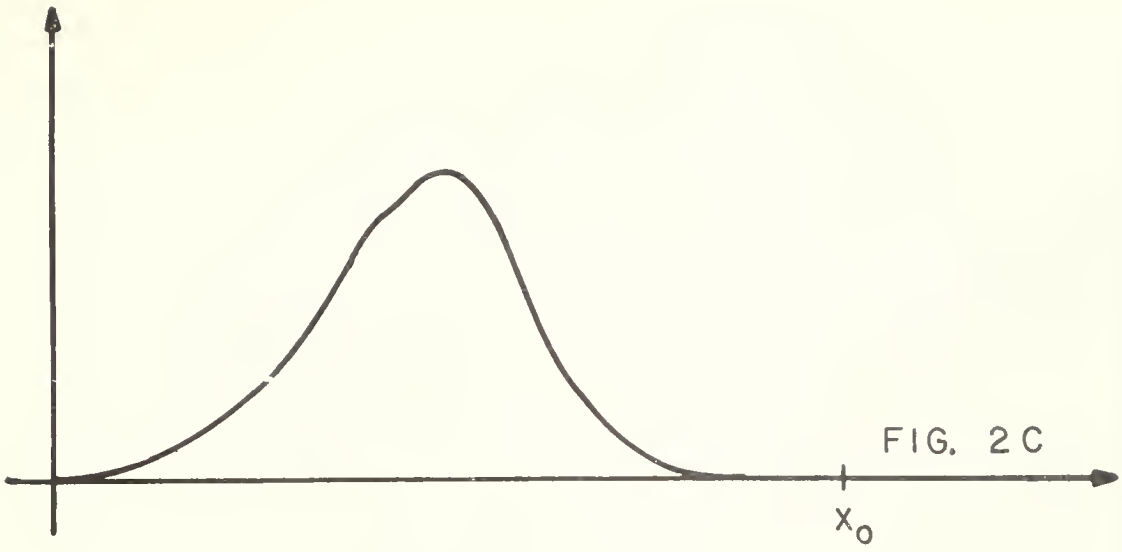

FIG. 2C

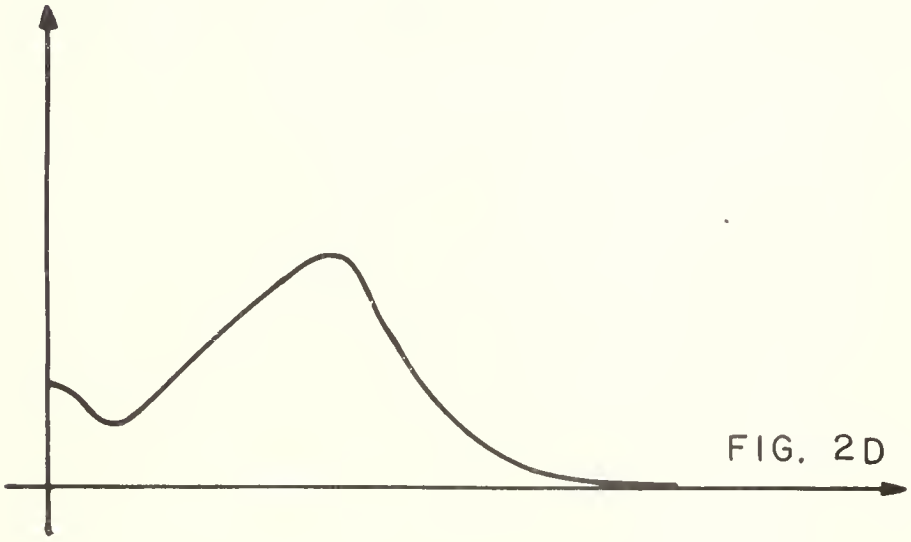

FIG. 2D

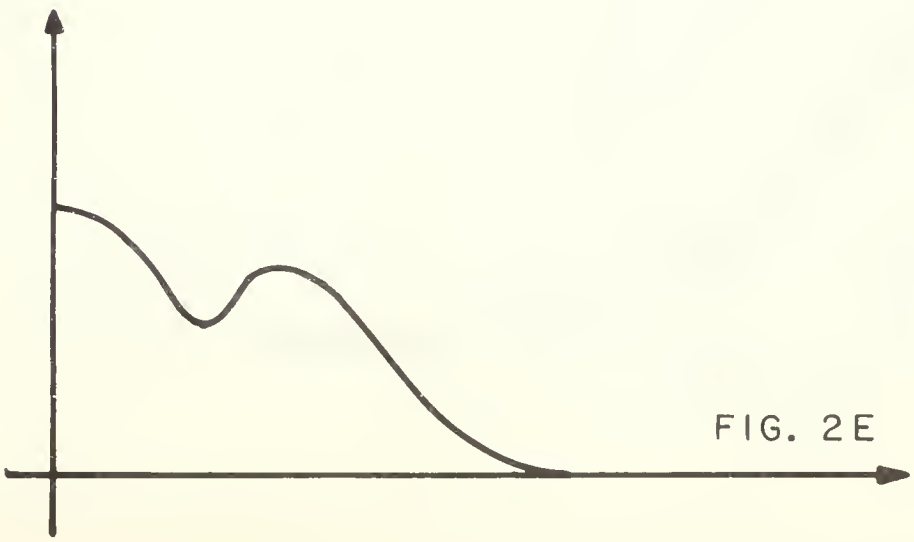

FIG. 2E

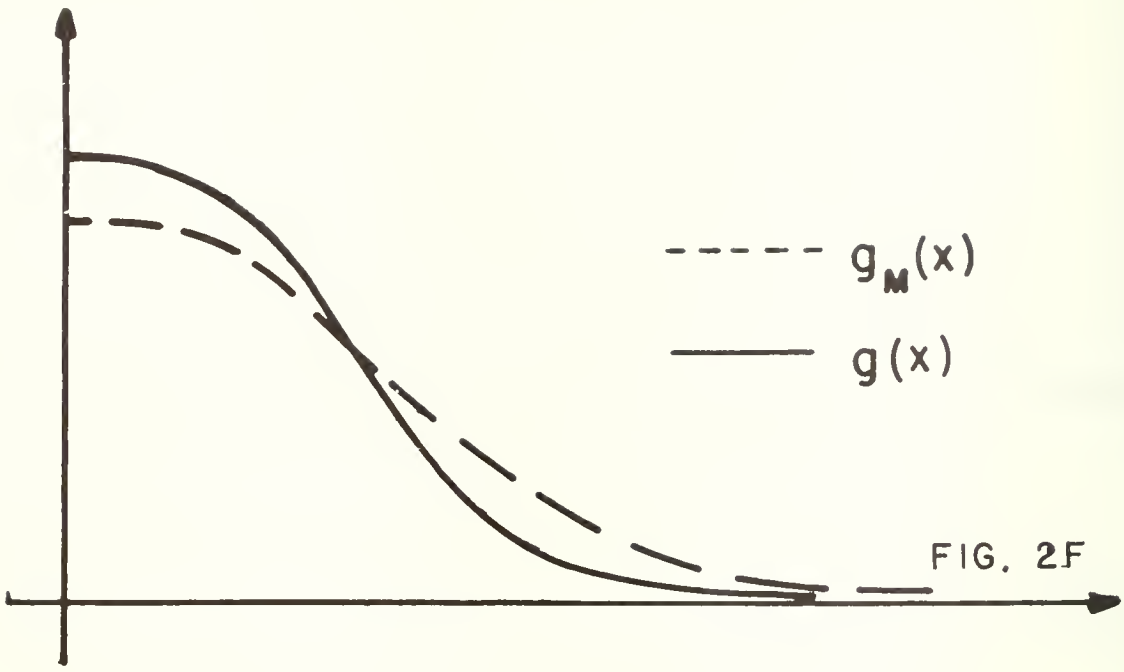

FIG. 2F

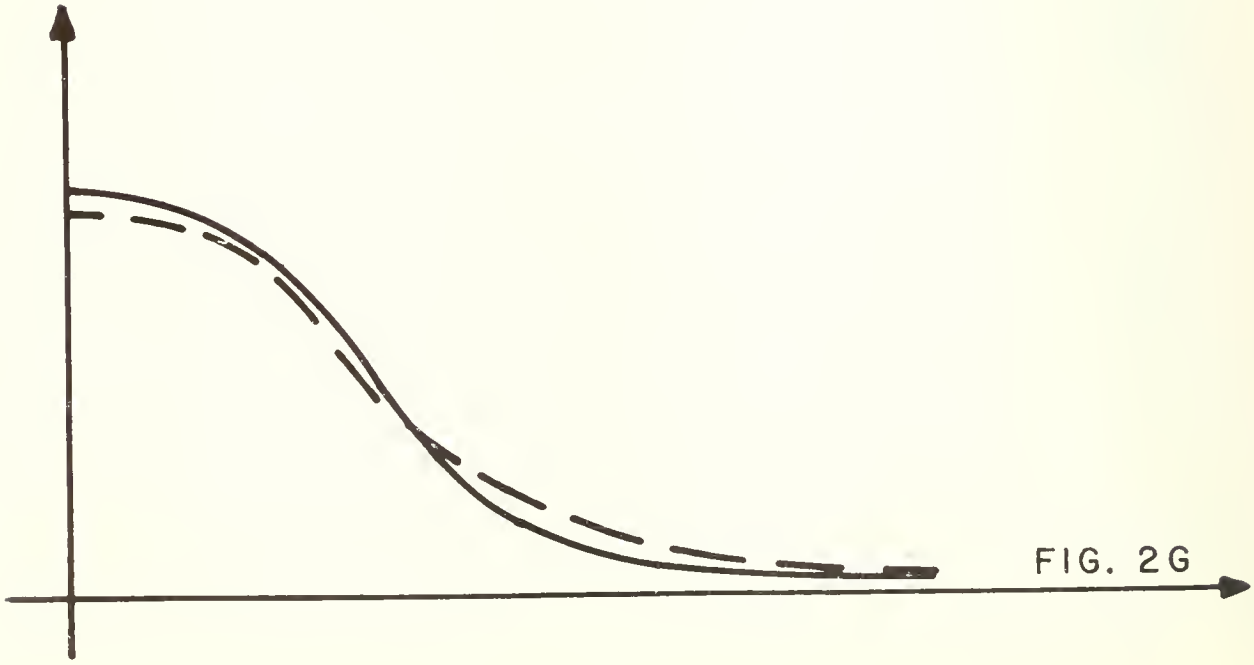

FIG. 2G

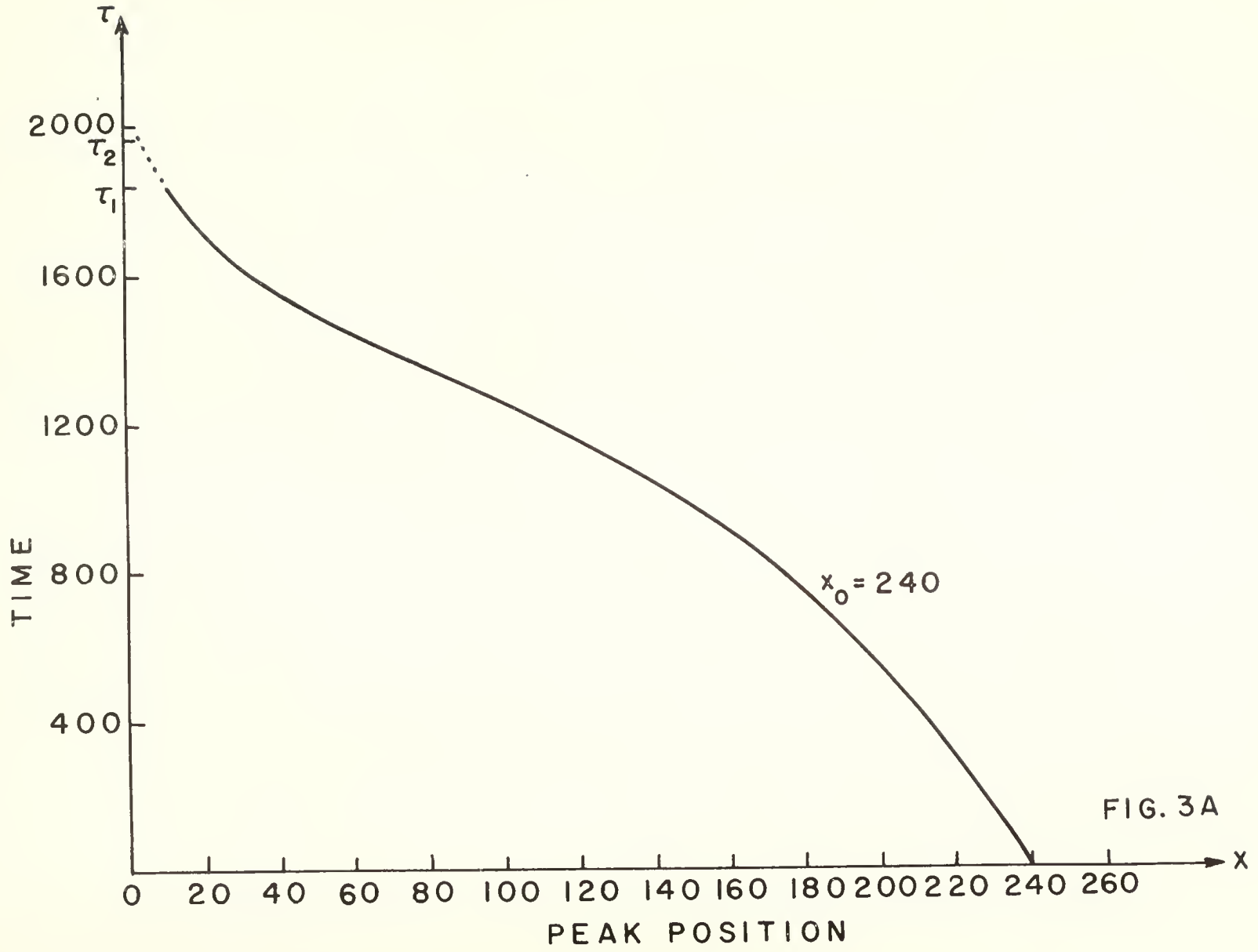
τ
2000
τ2
τ1
1600
1200
800
400
TIME
x0 = 240
0 20 40 60 80 100 120 140 160 180 200 220 240 260
X
PEAK POSITION

FIG. 3A

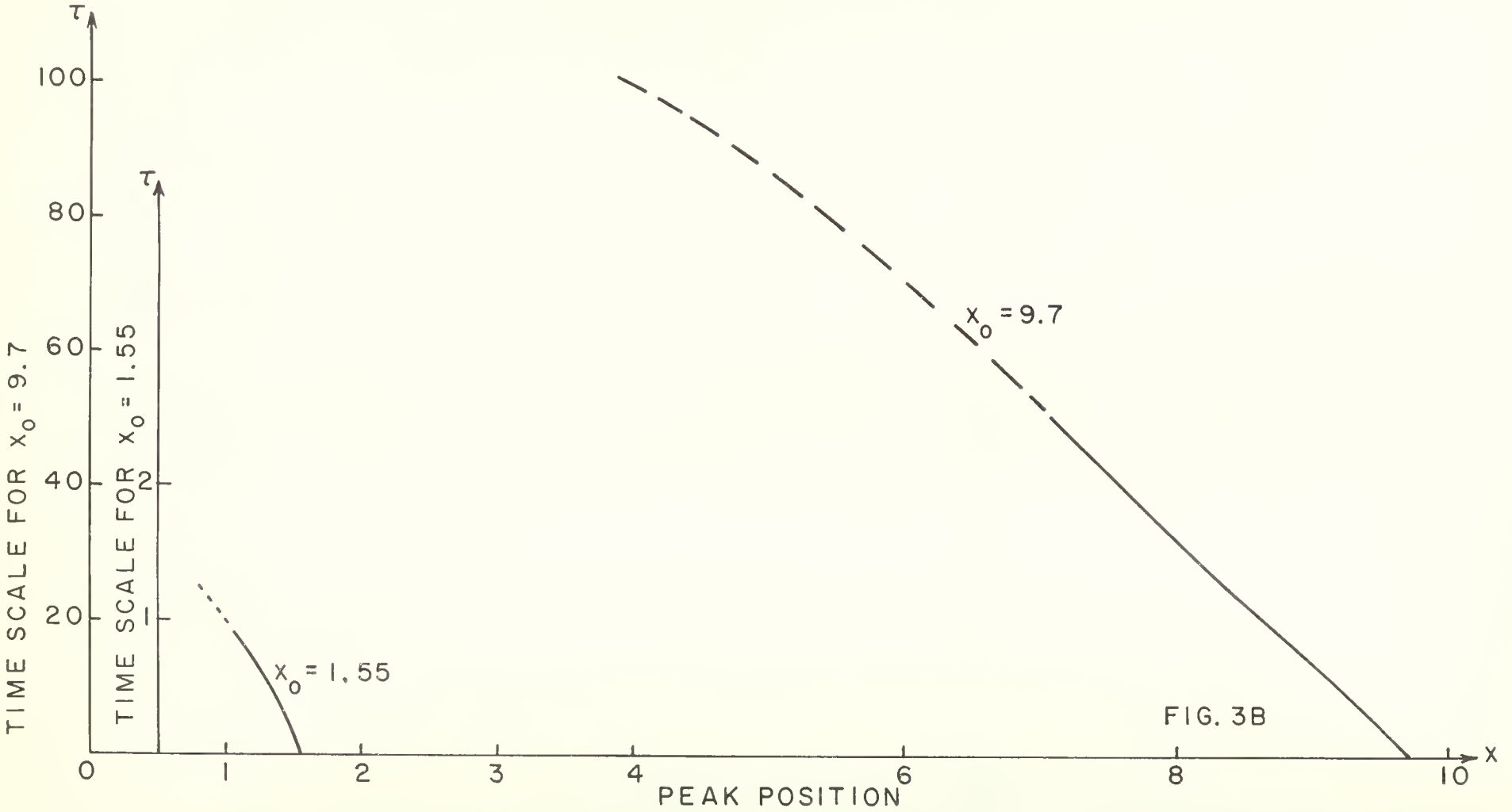
τ
100
80
60
40
20
TIME SCALE FOR $x_0 = 9.7$
τ
2
1
TIME SCALE FOR $x_0 = 1.55$
$x_0 = 9.7$
$x_0 = 1.55$
0
1
2
3
4
6
8
10
X
PEAK POSITION

FIG. 3B

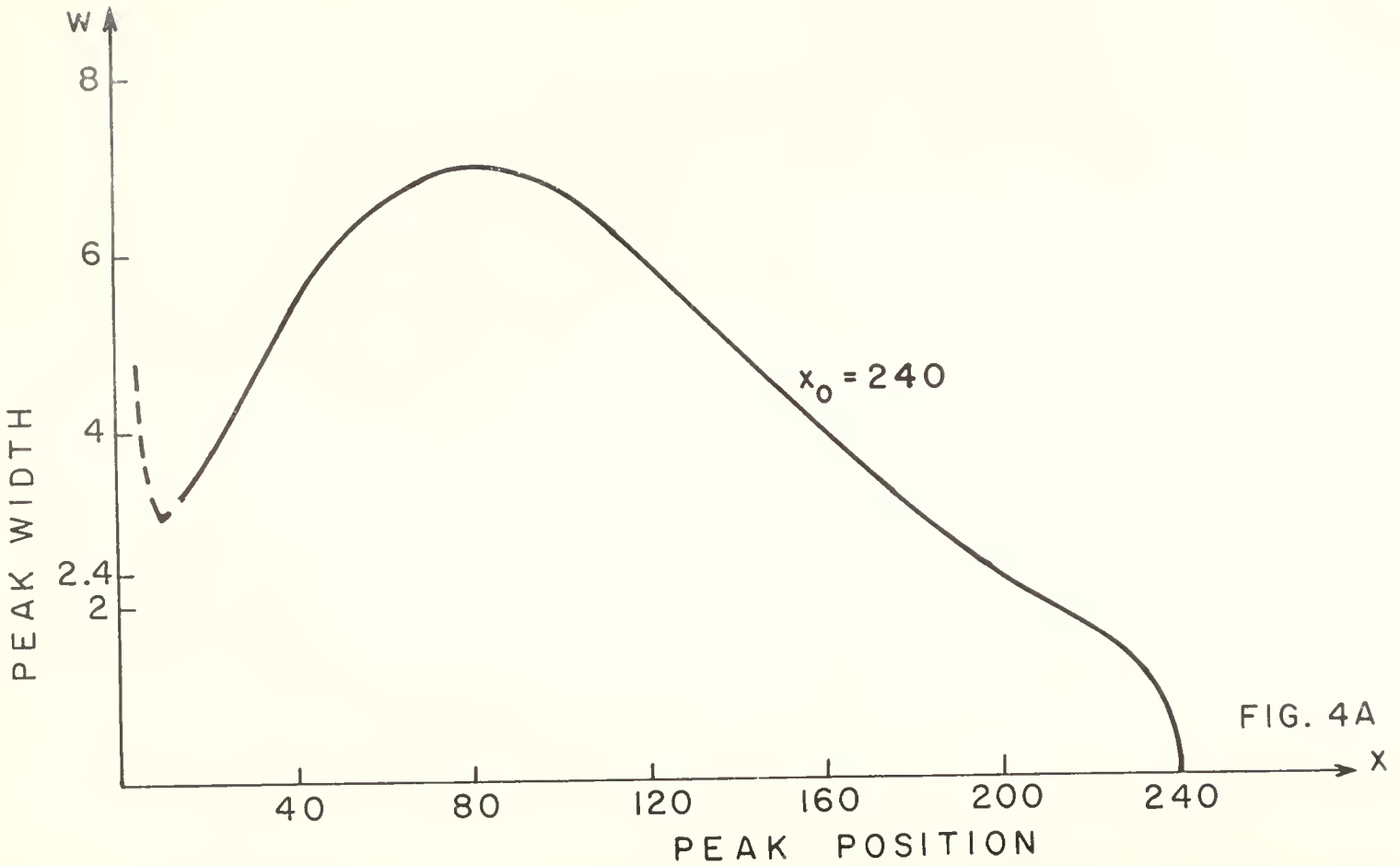
W
8
6
4
2.4
2
PEAK WIDTH
$x_0 = 240$
40
80
120
160
200
240
X
PEAK POSITION

FIG. 4A

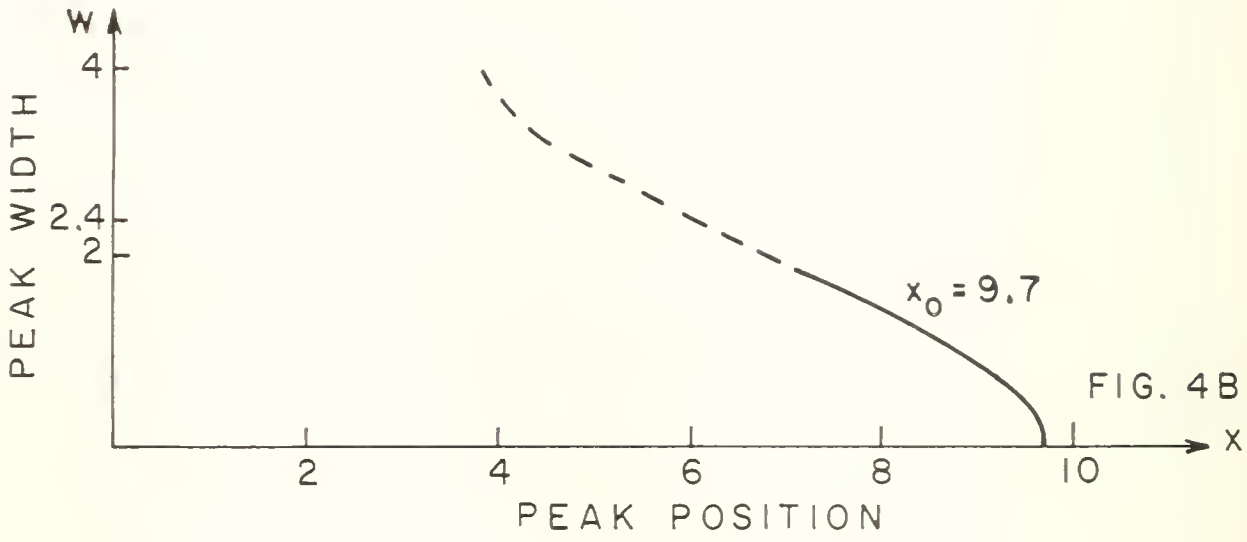

FIG. 4B

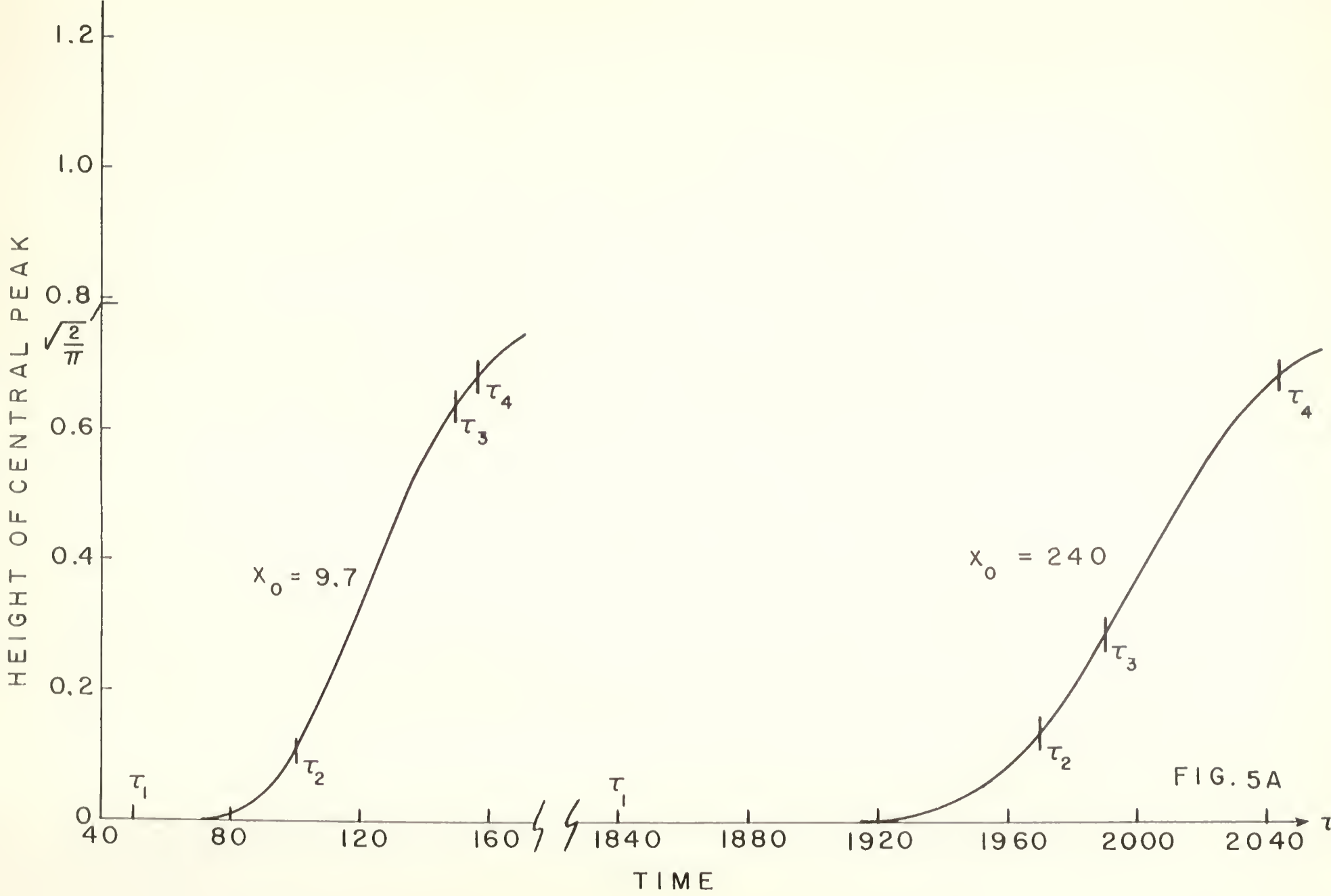
HEIGHT OF CENTRAL PEAK
1.2
1.0
0.8
$\sqrt{\frac{2}{\pi}}$
0.6
0.4
0.2
0
$X_0 = 9.7$
$X_0 = 240$
τ_1
τ_2
τ_3
τ_4
40
80
120
160
1840
1880
1920
1960
2000
2040
TIME

FIG. 5A

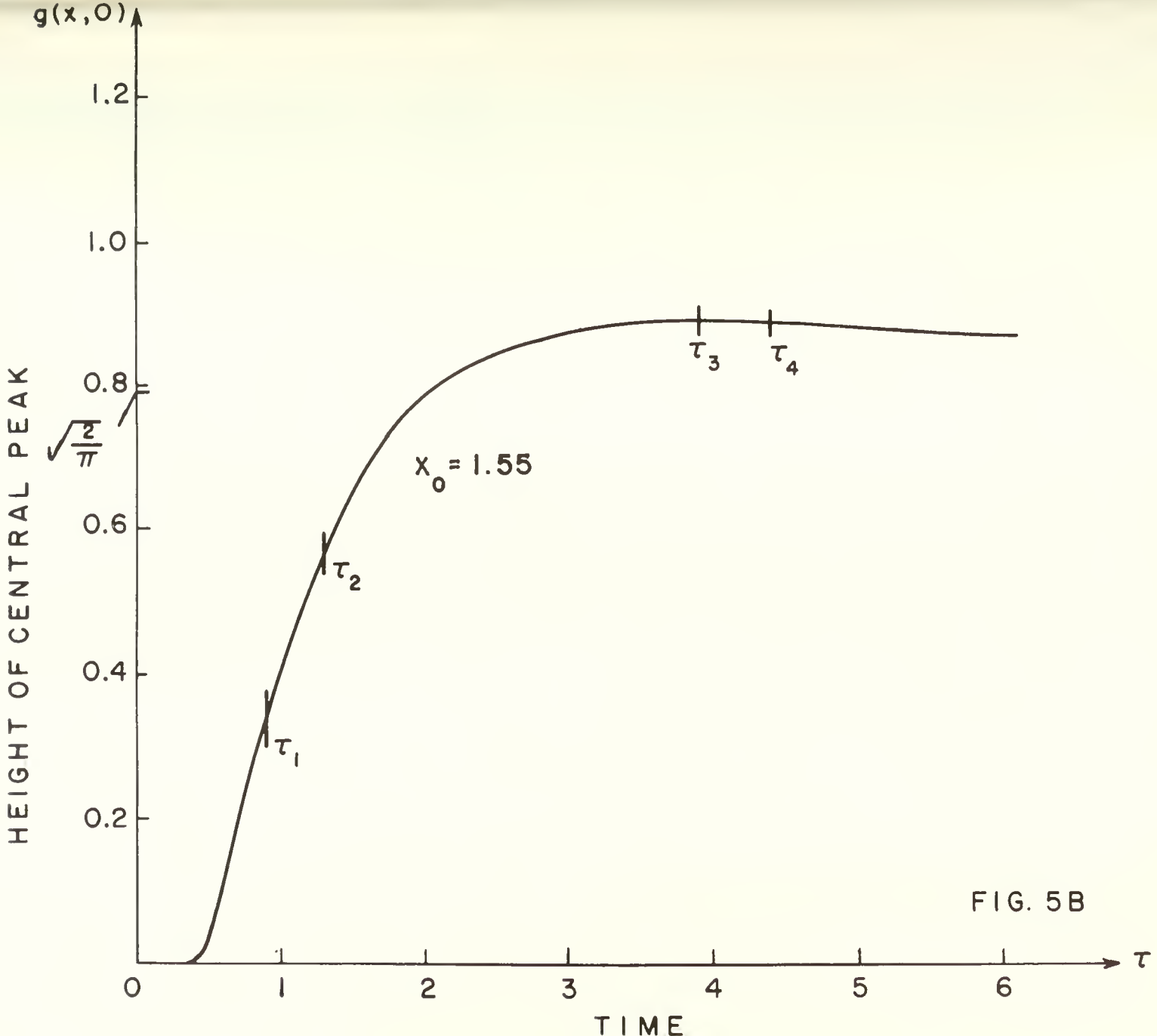
g(x,0)
1.2
1.0
0.8
0.6
0.4
0.2
HEIGHT OF CENTRAL PEAK
$\sqrt{\frac{2}{\pi}}$
$X_0 = 1.55$
τ_1
τ_2
τ_3
τ_4
0
1
2
3
4
5
6
τ
TIME

FIG. 5B

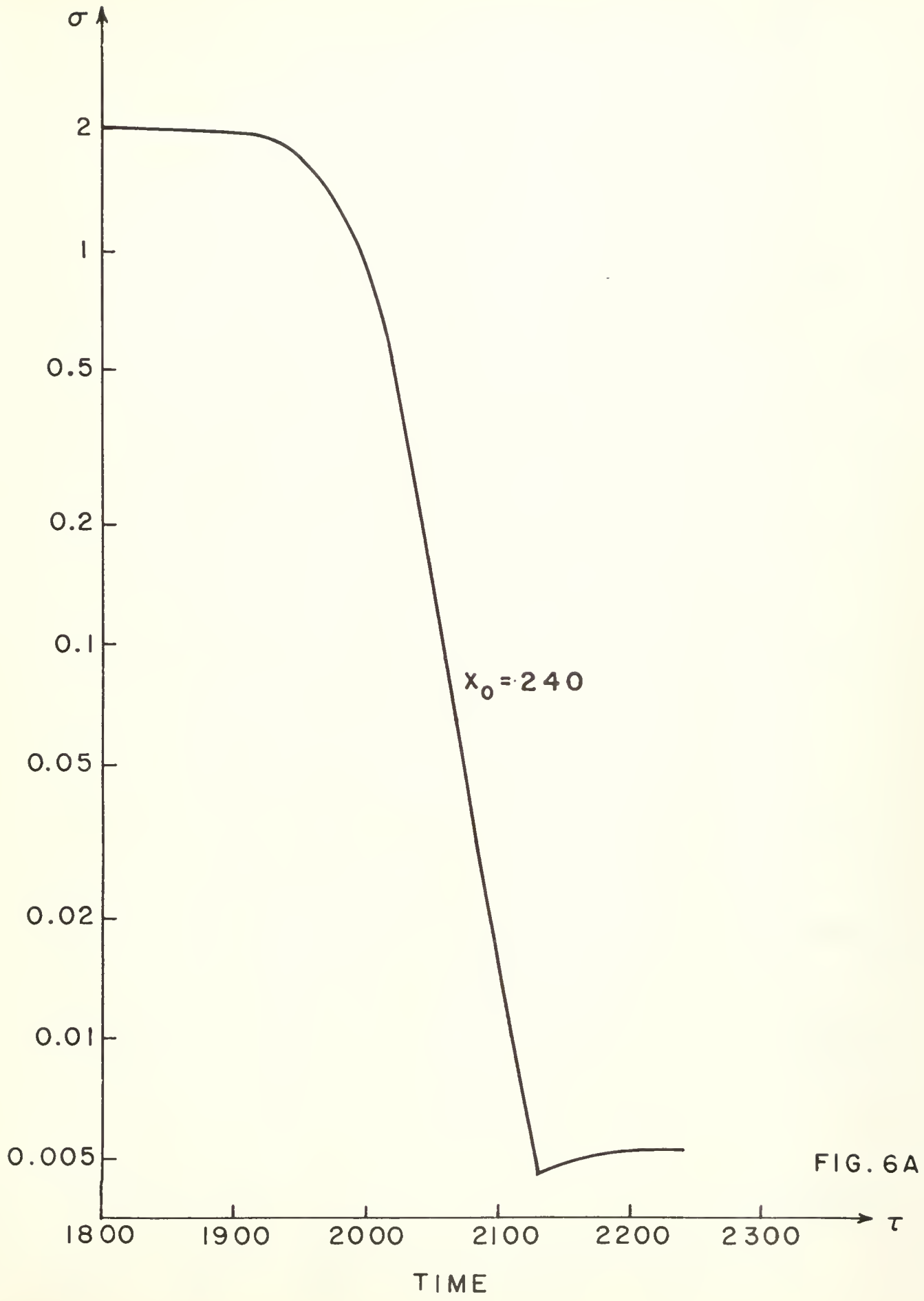
σ
2
1
0.5
0.2
0.1
0.05
0.02
0.01
0.005
$x_0 = 240$
1800
1900
2000
2100
2200
2300
τ
TIME

FIG. 6A

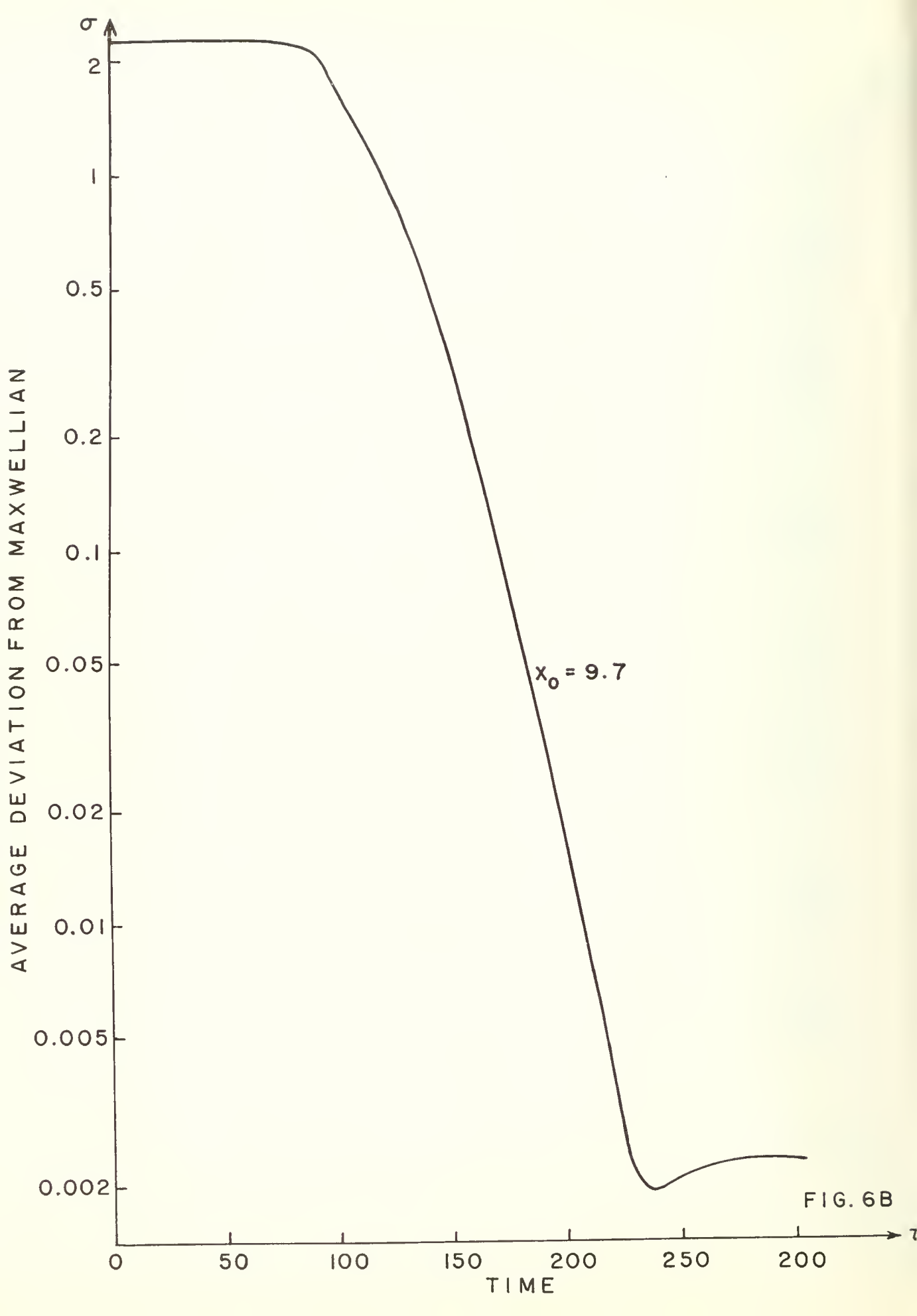
σ
2
1
0.5
0.2
0.1
0.05
0.02
0.01
0.005
0.002
AVERAGE DEVIATION FROM MAXWELLIAN
$x_0 = 9.7$
0
50
100
150
200
250
200
TIME
τ

FIG. 6B

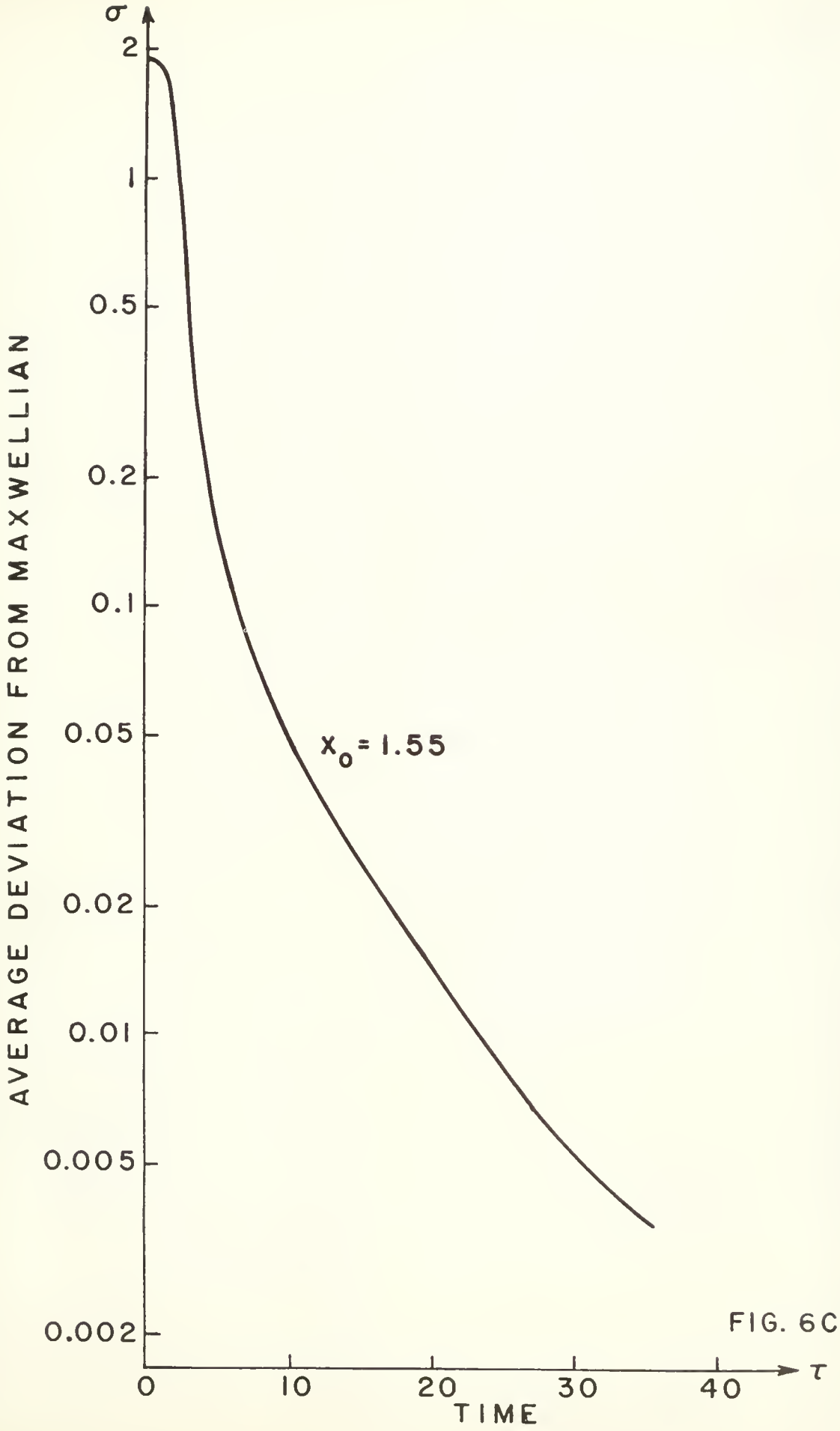
σ
2
1
0.5
0.2
0.1
0.05
0.02
0.01
0.005
0.002
AVERAGE DEVIATION FROM MAXWELLIAN
$x_0 = 1.55$
0
10
20
30
40
τ
TIME

FIG. 6C

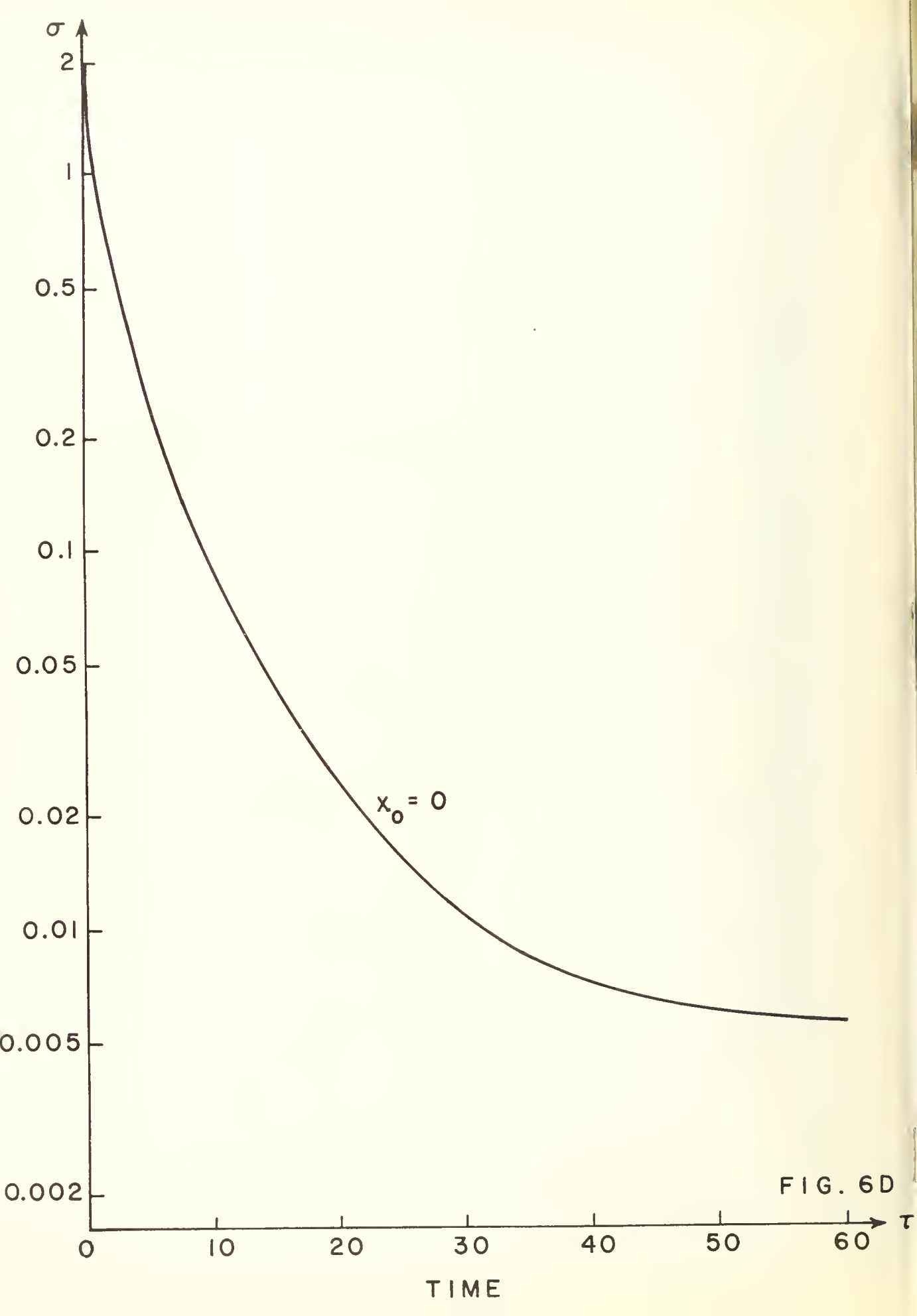

FIG. 6D